

# Tailoring Multilevel-Stable Remanence States in Exchange-Biased System through Spin-Orbit Torque

Jijun Yun, Qiaoning Bai, Ze Yan, Meixia Chang, Jian Mao, Yalu Zuo, Dezheng Yang, Li Xi,\* and Desheng Xue

Multilevel remanence states have potential applications in ultra-high-density storage and neuromorphic computing. Continuous tailoring of the multilevel remanence states by spin-orbit torque (SOT) is reported in perpendicularly magnetized Pt/Co/IrMn heterostructures. Double-biased hysteresis loops with only one remanence state can be tuned from the positively or negatively single-biased loops by SOT controlled sign of the exchange-bias field. The remanence states associated with the heights of the sub-loops are continually changed by tuning the ratio of the positively and negatively oriented ferromagnetic domains. The multilevel storage cells are demonstrated by reading the remanent Hall resistance through changing the sign and/or the magnitude of current pulse. The synaptic plasticity behaviors for neuromorphic computing are also simulated by varying the remanent Hall resistance under the consecutive current pulses. This work demonstrates that SOT is an effective method to tailor the remanence states in the double-biased heavy metal/ferromagnetic/antiferromagnetic system. The multilevel-stable remanence states driven by SOT show potential applications in future multilevel memories and neuromorphic computing devices.

## 1. Introduction


Multilevel states have attracted extensive attention because they could increase the storage density and/or reduce the integration complexity through storing multiple bits per cell.<sup>[1–3]</sup> This multilevel memory behavior can also be utilized for mimicking the function of synapses, which is significant for the neuromorphic computing systems.<sup>[4–6]</sup> In resistance change memory, several physical effects can be harnessed for realizing multilevel storage: phase changes,<sup>[5]</sup> atomic displacements,<sup>[6]</sup> reduction–oxidation phenomena.<sup>[7]</sup> Recently, big progress has been made in controlling the multilevel states based on the antiferromagnetic (AFM) and ferromagnetic (FM) materials. In a single AFM layer, which is immune to the external field due to the zero-net

magnetization, multilevel stable states have been achieved through electrical means,<sup>[8–10]</sup> while the readout signals are based on the anisotropic magnetoresistance of AFM. In the FM/heavy metal (HM) bilayer, a complete magnetization switching could be realized when the current density ( $J$ ) exceeds the critical current density ( $J_c$ ) based on the spin-orbit torque (SOT).<sup>[11–13]</sup> It was found that the multilevel states with relatively large Hall resistance as readout signal could be achieved at  $J < J_c$  through the incomplete switching of FM layer magnetization.<sup>[14,15]</sup> However, multilevel states could be more easily influenced by external field. If one combines the advantages of both AFM and FM systems, more significant and stable multilevel states in FM/AFM bilayers are naturally expected.

An AFM layer in conjunction with a FM layer will induce an exchange-bias effect, which is usually characterized as a shift of the hysteresis loop along the magnetic field axis.<sup>[16–19]</sup> In some exchange-biased systems, double-biased hysteresis loops<sup>[20–25]</sup> were observed rather than the usually observed single-biased loop. This interesting phenomenon, often observed in a demagnetized sample after zero field cooling or in as-deposited FM/AFM bilayers, arises from the coexistence of the oppositely oriented magnetic domains.<sup>[21–23]</sup> In this system, the double-biased hysteresis loop could be designed to have only one remanence state if the exchange-bias field is large enough and the coercivity is rather small. Thus, multilevel storage based on the remanence ratio could be realized by an appropriate method through continuously tailoring the heights of the sub-loops. However, for a FM/AFM system it is still challenging to effectively control the number of remanence states in order to enable it as a multilevel storage device.

The SOT effect has been demonstrated as an efficient way to switch the magnetization of FM or AFM, and was widely investigated owing to its potential applications in magnetic random access memory (MRAM) and other spintronic devices.<sup>[11–13,26–30]</sup> In particular, in HM/FM/AFM trilayers, Lin et al. recently reported that the hysteresis loops between positively and negatively single-biased loops could be manipulated by SOT through switching the FM spins and AFM interfacial spins completely and simultaneously with magneto-optical Kerr techniques.<sup>[31]</sup> It provides an effective approach to manipulate the FM magnetization and AFM interfacial spins in HM/FM/AFM

J. Yun, Q. Bai, Z. Yan, M. Chang, J. Mao, Prof. Y. Zuo, Prof. D. Yang, Prof. L. Xi, Prof. D. Xue  
Key Laboratory for Magnetism and Magnetic Materials of the Ministry of Education and School of Physical Science and Technology  
Lanzhou University  
Lanzhou 730000, P. R. China  
E-mail: xili@lzu.edu.cn

 The ORCID identification number(s) for the author(s) of this article can be found under <https://doi.org/10.1002/adfm.201909092>.

DOI: 10.1002/adfm.201909092

trilayers by SOT. One can speculate that the positively or negatively single-biased loop will be changed to a double-biased loop if the partial FM/AFM magnetization is switched by adjusting the current density smaller than  $J_C$ . Thus, the multilevel remanence states in the HM/FM/AFM system could be realized by tuning the heights of sub-loops through controlling the strength of SOT. Thanks to the insensitivity of AFM moments to magnetic fields, the multilevel states realized in the HM/FM/AFM system, in which the readout signal is based on the anomalous Hall resistance, will show the stable characteristic. Up to date, the multilevel remanence states, based on the HM/FM/AFM system, tailored by SOT have not been investigated.

In this work, we present continuously tunable hysteresis loops in HM/FM/AFM trilayers from the negatively single-biased loop to the double-biased loops, and finally to the positively single-biased loop by current-generated SOT using the Hall resistance as an indicator of the variation of magnetization. Furthermore, continuous tuning of the dual loop heights (magnetization amplitudes) and the associated remanence can be easily achieved by changing the current density and/or the in-plane field. Magneto-optical Kerr microscope was also used to record the hysteresis loops and the evolution of magnetic domains at the Hall cross after the action of current-induced SOT. The domain images directly show that the multilevel remanence states are dominantly governed through domain wall motion by SOT. Besides, the evolution of stable multilevel remanent Hall resistance with the consecutive current pulses in the Pt/Co/IrMn stacks can be viewed as the plasticity of a synapse, which is significant for neuromorphic system.

The method of SOT-controlled multilevel states in this work could pave a way to achieve the tunable multilevel-stable remanent Hall resistance for potential application in the multilevel storage and the neuromorphic computing system.

## 2. Results and Discussions

### 2.1. Measurement Configuration and SOT Induced Reversal of Exchange-Bias

The film stacks of Ta(2.6)/Pt(5.5)/Co(0.8)/Ir<sub>20</sub>Mn<sub>80</sub>(6.2)/Ta(1.3)/TaO<sub>x</sub>(1.6) (thickness in nm) were designed to show the large exchange-bias field and perpendicular magnetic anisotropy (See details in Supporting Information S1). The layer by layer structure of our sample was verified via grazing incidence X-ray reflectivity (XRR) measurements. The XRR pattern was simulated by GenX program<sup>[32,33]</sup> and shown in Figure 1a. The simulated depth profile of X-ray scattering length density (SLD) indicates the well-defined structures with quite small roughness of each layer. Then the films were patterned into 10  $\mu\text{m}$  wide Hall bars as shown in Figure 1b for magnetotransport measurements. The hysteresis loop was characterized either by the anomalous Hall resistance or by the domain contrast, with a typical double-biased loop shown in Figure 1c. The origin of the double-biased loop is from the coexistence of up and down magnetized Co sub-domains, which are coupled with IrMn and have opposite exchange-bias fields in each domain (see details in

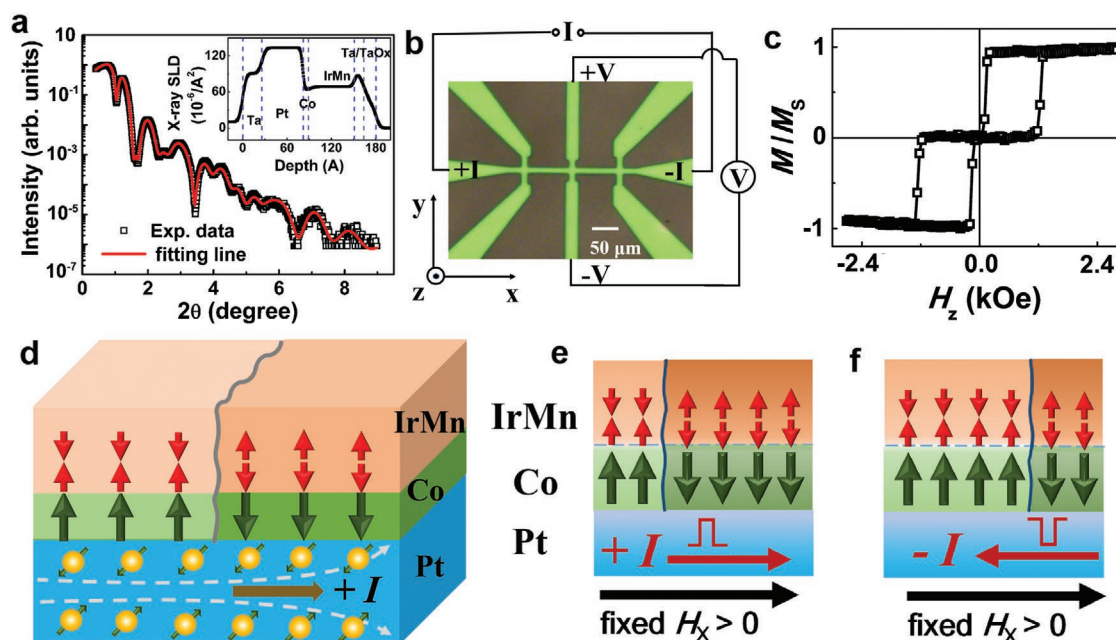


**Figure 1.** Sample structure and measurement schematic. a) X-ray reflectivity data of the Pt/Co/IrMn sample. Black squares are experimental data and the red solid line is the fitting curve. The inset in a) is the depth profile of X-ray scattering length density (SLD) for the sample. b) Optical image of the Hall bar and measurement configuration. c) The typical double-biased hysteresis loop characterized by the anomalous Hall resistance or the domain contrast. d) Schematic of the studied Pt/Co/IrMn system and the spin-transport process under a current along the x axis. Green and red arrows represent the magnetic moments in Co layer and IrMn interfacial spins, respectively. The light-colored area shows the up magnetized domain, while the dark-colored area shows the down magnetized domain. The schematic domain area after e) a positive current pulse and f) a negative current pulse induced SOT in the presence of in-plane field  $H_x$ .

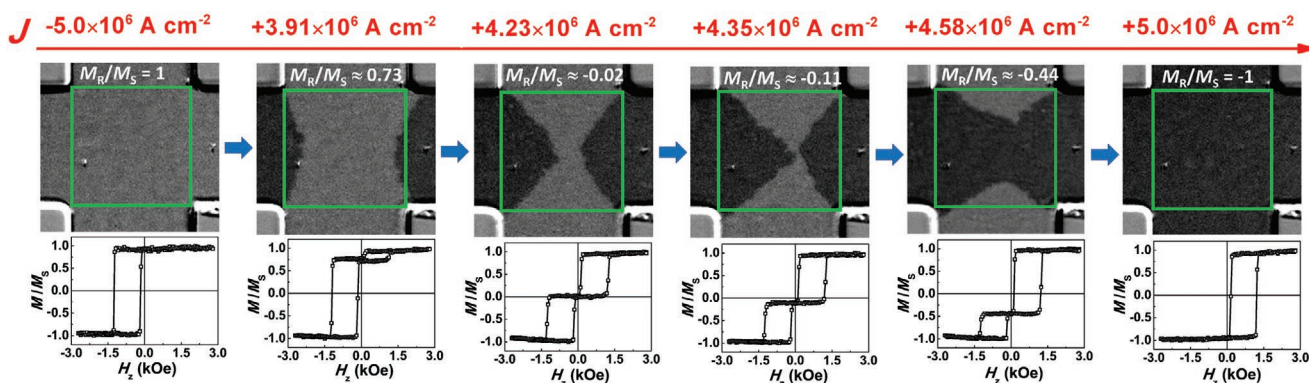


**Figure 2.** Evolution of remanent magnetic domains in Hall cross (green block) with the current density changing. The magnetic domain images were taken by Kerr Microscope after applying current pulses, and the corresponding hysteresis loops are also shown below the images.

Supporting Information S2). Figure 1d shows the schematic of the studied Pt/Co/IrMn system and spin-transport process under a current along the  $x$  axis. When a current is passed through the Pt layer, a spin current will be generated in the  $z$  direction due to the spin Hall effect (SHE),<sup>[11–13]</sup> which will exert a SOT on the magnetization. Afterwards, the FM magnetization can be switched by the SOT with the assistance of an in-plane field  $H_x$ . Then, the AFM interfacial spins disturbed by the current-generated SOT tend to align with the FM magnetization.<sup>[31]</sup> Thus, not only the magnetization but also the exchange-bias are reversed by SOT. Due to the deterministic magnetization switching by SOT,<sup>[11–13,26–30]</sup> only the up (down) magnetized domain could be switched to opposite direction under a positive (negative) current pulse with an assistance field of  $+H_x$ , as schematically shown in Figure 1e,f. Thereby, concurrent switching of FM magnetization and AFM interfacial spins by SOT can be realized. In Pt/Co/IrMn trilayers, the SOT efficiency with damping-like effective field per unit current density is determined to be  $10.06 \text{ Oe}/(10^6 \text{ A cm}^{-2})$  by the harmonic Hall voltage measurement method (see details in Supporting Information S3). When the magnitude of current pulse reaches  $\pm 6.10 \times 10^6 \text{ A cm}^{-2}$ , the strong SOT could fully tune the exchange-bias fields between positive and negative values in Pt/Co/IrMn trilayers with single-biased hysteresis loop. Thanks to the large exchange-bias field and small coercivity, the remanence shows a single value. Thus, the two stable reversible remanence states can be achieved by changing the polarity of the currents (see details in Supporting Information S4).

For the SOT induced magnetization switching in the HM/FM systems, domain nucleation and domain wall motion are the dominant process.<sup>[12–14]</sup> If the amplitude of current density  $J$  is less than  $J_C$  (defined as the smallest current density required to completely switch the FM magnetization), there will be an incomplete switching of FM magnetization.<sup>[13,14]</sup> In HM/FM/AFM trilayers, if the partial FM magnetization is switched, the height of the positive (negative) biased loop will be changed since the AFM interfacial spins will also be switched to align with the FM magnetization. Thus, the change of the remanence and the heights of the sub-loops in HM/FM/AFM trilayers could be delicately designed and realized by controlling the strength of SOT.

## 2.2. Tailoring Double-Biased Hysteresis Loops through SOT

The partial switching of FM magnetization and the associated evolution of double-biased hysteresis loop through SOT is indeed observed in Pt/Co/IrMn trilayers by applying a current with  $J < J_C$  in a specific assistant field  $H_x$ . To give an insight into the magnetic domain states associated with the evolution of hysteresis loops, magneto-optical Kerr microscope measurements<sup>[34,35]</sup> were taken on the Hall bar device. Pulse currents with different amplitudes were firstly applied to achieve different remanent states. It is found that the magnetic domains are nucleated firstly in the current line of the Hall bar after applying current pulses. Then the domains expand along the current direction, which is consistent with previous reports about current induced domain wall motion<sup>[12,14]</sup> (See details in Supporting Information S5). Then we mainly focused on the variation of magnetic domain in the cross area because the detected Hall voltage is determined by the domain configuration in the Hall cross. The evolution of magnetic domain images in the Hall cross and the corresponding hysteresis loops under various current densities are shown in Figure 2. When the remanence ratio of  $M_R/M_S$  is  $\pm 1$ , there is a single magnetic domain state where magnetization points to “up” or “down”. If  $M_R/M_S$  is not  $\pm 1$ , the remanent domains consist of spatially separated subsystems, in which the remanent magnetization points opposite to each other. With the positive current density increasing, it is obvious that the “dark grey” domain (represents  $M$  in “down” state) grows increasingly, while the “light grey” domain shrinks and finally vanishes. And the area ratio of the “dark grey” and “light grey” domains varies with the remanence changing. It is because that the SOT determines the switching of FM magnetization and then it disturbs the AFM interfacial spins to align with the FM magnetization. Thus, with the increase in positive current, more FM moments will be switched to “down” state under the positive  $H_x$ , and the AFM interfacial spins will also be switched to “down” state. So, the domain image will show a bigger “dark grey” area after applying positive current pulses. The unique behavior of domain wall motion in the Hall cross can be explained by the current shunting effect.<sup>[36]</sup> Under the action of an applied current, there exists the distribution of current density in the Hall cross. So, when applying a current pulse, the magnetic



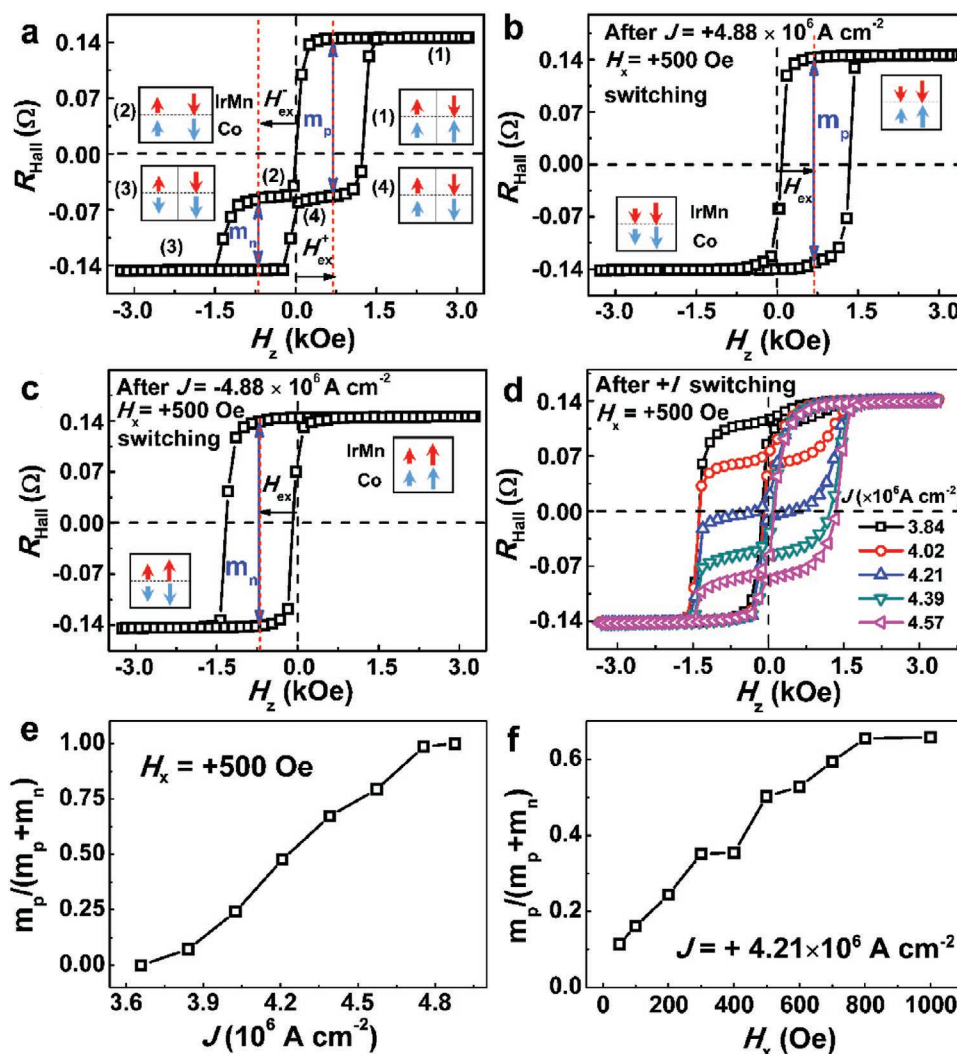


**Figure 3.** Tailoring double-biased hysteresis loops by SOT. a–c) Anomalous Hall hysteresis loops for the sample a) in the as-deposited state, after b) positive, and c) negative current switching with amplitude of  $4.88 \times 10^6 \text{ A cm}^{-2}$  under in-plane field  $H_x = +500 \text{ Oe}$ . Different schematic configurations for the Co moments (blue arrows) and IrMn interfacial spins (red arrows, only the nearest IrMn spins in contact with Co are drawn) at different stages are shown. The  $m_p$  and  $m_n$  values defined in the (a–c) signify the magnetization of the positive and negative biased loops, respectively. d) Hysteresis loops after positive current induced SOT switching with different current densities under  $H_x = +500 \text{ Oe}$ . e) Current density  $J$  dependence of  $m_p/(m_p + m_n)$  for the hysteresis loops, which measured after SOT switching with different current densities under  $H_x = +500 \text{ Oe}$ . f)  $H_x$  dependence of  $m_p/(m_p + m_n)$  for the hysteresis loops, which measured after SOT switching with  $J = +4.21 \times 10^6 \text{ A cm}^{-2}$  under different  $H_x$ .

moments will first reverse in this area where the current density is larger. Moreover, the exchange-bias field obtained from hysteresis loops does not change, as shown in Figure 2. It indicates the exchange coupling constant between Co and IrMn is insensitive to the SOT strength. In addition, the hysteresis loops were also measured on the “dark grey” and “light grey” areas when  $M_R/M_S \neq \pm 1$  (see details in Supporting Information S2). One can see that the hysteresis loops in the “dark grey” and “light grey” areas show positive and negative exchange-bias, respectively. The Kerr microscope measurements reveal that the heights of the sub-loops can be tuned by SOT and the remanent domain images cannot be erased by magnetic field. The evolution of domain image in the Hall cross demonstrates that the multilevel remanence can be realized by SOT through domain wall motion.

Given that the readout of multilevel remanence states based on electrical signal is superior to that based on optical signal for application, we further studied the SOT induced remanence change in the double-biased loops using magnetotransport measurements. Figure 3a shows the Hall resistance loop for the Pt/Co/IrMn sample deposited without any magnetic field. The whole loop is divided into two sub-loops, which shift to opposite directions with the same amplitude of the exchange-bias fields  $H_{\text{ex}}$  around 690 Oe due to the same interface-determined exchange coupling effect between Co and IrMn. The heights of the two sub-loops are not the same, which means unequally pinned magnetization of Co by positive and negative  $H_{\text{ex}}$ . This phenomenon is mainly caused by the non-uniform stray field generated from the magnets in the magnetron sputtering guns.<sup>[25,37]</sup> Since the double-biased loops originate from

the coexistence of up and down domains, arrows representing magnetization in each domain in the specific points of a hysteresis loop are drawn and shown in Figure 3(a–c). The  $m_p$  and  $m_n$  are used to represent the height of the positive loop and that of the negative one, respectively. In Figure 3b, after the positive current ( $J \approx +4.88 \times 10^6 \text{ A cm}^{-2}$ ) applied under  $H_x = +500 \text{ Oe}$ , the Hall resistance loop changes from the as-deposited double-biased shape to a single-biased one with a positive  $H_{\text{ex}}$  around 690 Oe, owing to the deterministic SOT switching of the initially up-magnetized domains. By just reversing the polarity of the applied current (i.e.,  $J \approx -4.88 \times 10^6 \text{ A cm}^{-2}$ ), the strong SOT makes the positive-biased single loop change to a negative-biased one with nearly the same value of  $H_{\text{ex}}$ , which indicates that the down-magnetized domain switches to up-magnetized domain deterministically. Figure 3(a–c) confirms that no matter what the initial state is, complete switching of the AFM interfacial and FM spins occurs under the action of a strong SOT in Pt/Co/IrMn trilayers.

To testify the multilevel states based on remanent Hall resistance, the negative current was firstly applied with  $J \approx -4.88 \times 10^6 \text{ A cm}^{-2}$  under  $H_x = +500 \text{ Oe}$  to obtain the initial hysteresis loop as shown in Figure 3c. Then a series of positive currents were applied with different amplitudes under  $H_x = +500 \text{ Oe}$ . After each current-induced SOT switching, the loops are measured and summarized in Figure 3d. Obviously, the hysteresis loops with different  $m_p$  and  $m_n$  are obtained as expected. The results from the magnetotransport measurements are consistent with those via the magneto-optical Kerr microscope measurements. It should be mentioned that the evolution between the double-biased loops and the single-biased loop with either positive or negative  $H_{\text{ex}}$  can be achieved by only changing the magnitude and the polarity of the current density (see details in Supporting Information S6). In addition, for the SOT induced magnetization switching in the HM/FM systems, the partial switching of FM magnetization could be happened with the variation of  $H_x$  and fixing  $J$ . This phenomenon was also observed in our samples with the variation of  $H_x$  and fixing the current density  $J \approx +4.21 \times 10^6 \text{ A cm}^{-2}$ . Figure 3e,f show the summarization of the SOT induced height variation of sub-loops through changing either current density or the in-plane field. It shows that  $m_p/(m_p + m_n)$  can be continuously tuned with the increase in  $J$  when  $H_x$  is fixed and vice versa. Thus, our results demonstrate that SOT is a promising approach to tailor the heights of the sub-loops in the double-biased loops.

### 2.3. Tunable Multilevel-Stable Remanent Hall Resistance

It is remarkable that tailoring double-biased loops accompanied by the change of remanent magnetization will certainly tune the Hall resistance  $R_{\text{Hall}}$ . Therefore, one can make use of the Hall voltage as the readout signal to realize multilevel storage. Here, the magnetization was first set into the down state by a positive reset current pulse ( $J \approx +4.88 \times 10^6 \text{ A cm}^{-2}$ , pulse width  $\approx 100 \text{ ms}$ ) under  $H_x = +500 \text{ Oe}$ . Then, negative current pulses were applied with increase in their amplitudes under  $H_x = +500 \text{ Oe}$ . The value of  $R_{\text{Hall}}$  was recorded after outputting each current pulse and shown in Figure 4a. The  $R_{\text{Hall}}$  increases gradually with the increase in amplitude of these

negative current pulses and changes from  $-0.14$  to  $0.14 \text{ } \Omega$ . It demonstrates that multilevel switching can be realized and the Hall resistance levels are determined by the amplitude of the current pulse. Similarly,  $R_{\text{Hall}}$  gradually decreases from  $0.14$  to  $-0.14 \text{ } \Omega$  when the amplitude of positive current pulse increases as shown in Figure 4b. Afterwards, current pulses were applied with varied amplitudes and polarities to test whether arbitrary multilevel states can be realized. The  $R_{\text{Hall}}$  was firstly set to  $-0.14 \text{ } \Omega$  after applying a reset current pulse ( $J \approx +4.88 \times 10^6 \text{ A cm}^{-2}$ ). Then a series of current pulses were applied with alternating polarities and amplitudes. It is found that  $R_{\text{Hall}}$  increases (decreases) after applying a negative (positive) current pulse. In addition, when applying a current pulse identical to the previous one,  $R_{\text{Hall}}$  keeps nearly constant. It indicates that the current pulse width (100 ms) is long enough to ensure  $R_{\text{Hall}}$  is switched to a stable value. Moreover, the good stability is demonstrated by the unchanged value of  $R_{\text{Hall}}$  after applying an out-of-plane disturbing magnetic fields around  $\pm 2000 \text{ Oe}$ . Although the training effect<sup>[38,39]</sup> in the exchange-biased system will decrease the exchange-bias field, a weak training effect and almost unchanged remanence ratios are observed in our sample (see details in Supporting Information S7). Thus, the remanence states of the device are quite stable for data storage, and the magnetic states can only be changed when applying a current pulse. The results demonstrate that the storage cell with quite stable multi-states tailored by SOT can be realized in HM/FM/AFM trilayers.

### 2.4. Mimicking Synaptic Behaviors

One of the most important applications for multilevel storage is neuromorphic computing, in which artificial synapses are indispensable basic devices. Usually, the resistance variation induced by programming consecutive pulses sequences can be utilized to imitate the synaptic behaviors (e.g., to reproduce the plasticity of synapses).<sup>[4,5,40,41]</sup> Synaptic plasticity is the ability of synapses to reconfigure the strength with which they connect two neurons according to the past electrical activity of these neurons.<sup>[40,42]</sup> It allows neural networks to learn and form memories. Under an external stimulus, spikes or action potentials from the preneuron are transmitted through synapse to the postneuron and generate excitatory postsynaptic potentials (EPSP) or inhibitory postsynaptic potentials (IPSP), together with the synaptic weight updates.<sup>[42,43]</sup> The information storage and learning of human brains are exactly a consequence of changes in the synaptic weight. The evolution of stable multilevel remanent Hall resistance with the consecutive current pulses in the Pt/Co/IrMn stacks can be viewed as the plasticity of a synapse, which is illustrated in Figure 5. The magnetization was first set into the up state by a negative reset current pulse ( $J \approx -4.88 \times 10^6 \text{ A cm}^{-2}$ , pulse width  $\approx 100 \text{ ms}$ ) under  $H_x = +500 \text{ Oe}$ . Then, a series of 120 current pulses were applied with positive polarity (red points) and negative polarity (blue points) for different current amplitudes with a fixed pulse width of 1 ms, as shown in Figure 5a. Obviously,  $R_{\text{Hall}}$  gradually decreases (increases) and tends to saturate with the increasing number of positive (negative) current pulses. Besides, a series of 120 current pulses were applied with positive polarity

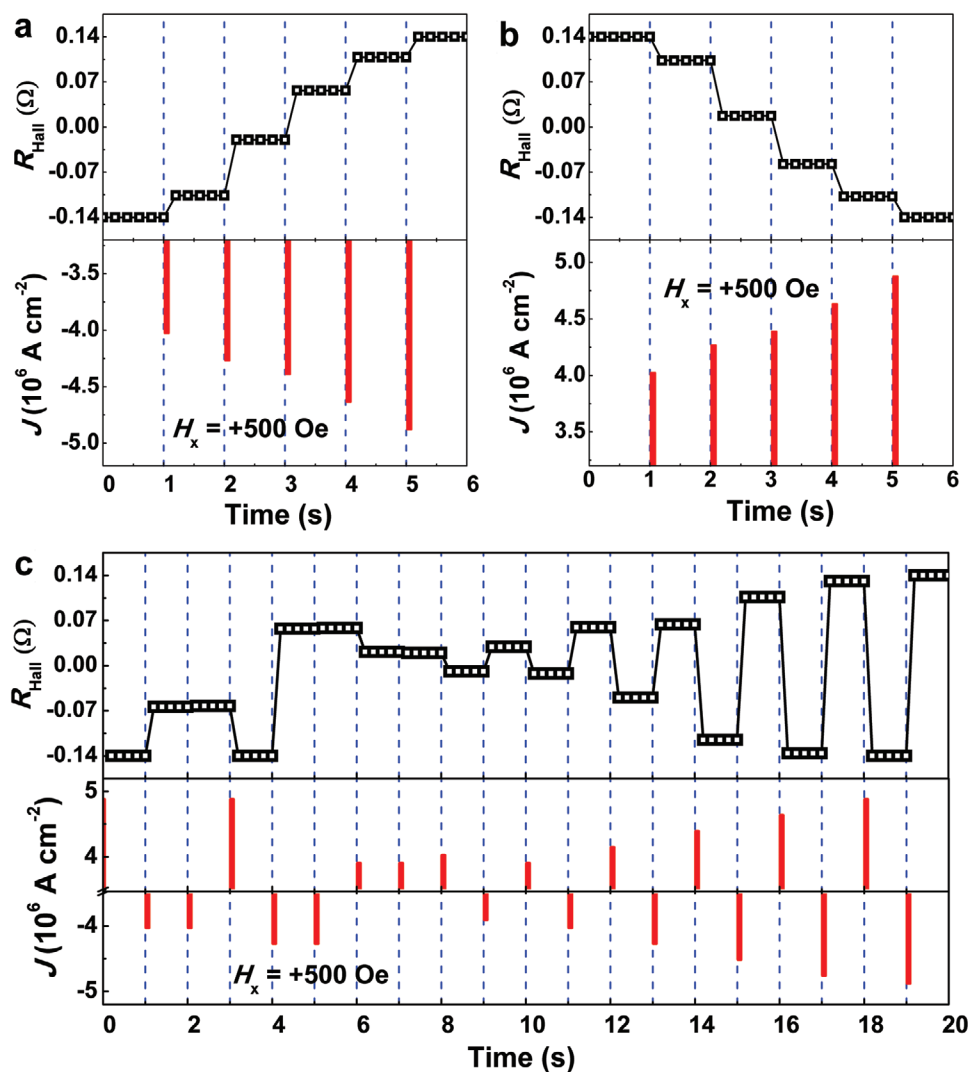


**Figure 4.** Tuning anomalous Hall resistance  $R_{\text{Hall}}$  by applying pulse current (pulse width 100 ms) under  $H_x = +500$  Oe.  $R_{\text{Hall}}$  responses to the a) negative and b) positive current density with increasing amplitudes. c) Multilevel  $R_{\text{Hall}}$  modulation resulting from the sequence of current density with alternating polarities and amplitudes.

(red points) and negative polarity (blue points) for different pulse widths with a fixed current amplitude, as shown in Figure 5b. Similarly,  $R_{\text{Hall}}$  gradually varies with the increasing numbers of pulses. Here, the artificial synapse is achieved by regarding the  $R_{\text{Hall}}$  value as the synaptic weight, which can be modulated by the applied current pulses. Therefore, the increase and decrease in  $R_{\text{Hall}}$  value, as shown in Figure 5, can be treated as the synaptic plasticity behaviors of EPSP and IPSP, respectively. Moreover, the variation magnitude of  $R_{\text{Hall}}$  after 120 number of pulses is larger either for the larger amplitude of current pulse or for the longer pulse width. The evolution of  $R_{\text{Hall}}$  is analogous to a synaptic behavior, in which a stronger or longer-time stimulus leads to the larger variation of synaptic weight. In particular, the remanent  $R_{\text{Hall}}$  states in the Pt/Co/IrMn stacks are quite stable with time. So the EPSP and IPSP can be classed as long-term plasticity.<sup>[5,14,43]</sup> It should be mentioned that the incomplete switching of magnetization in HM/FM bilayers by SOT can also be used for multilevel memory

and neuromorphic computing.<sup>[14,15]</sup> However, the magnetic state could be easily changed by external magnetic field. The advantage of our devices is quite stable, which endows the ultra-high-density neuromorphic computing network with improved stability for data processing and storage.

It should be mentioned that further investigation for multilevel memory is needed for the integration of our sample in magnetic tunnel junctions (MTJs) to magnify the output multilevel signal and the realization of field-free SOT tailoring. At this stage, it needs more subsequent experiments to check the possibility. However, some reports may provide the theoretical possibility. For example, Kim et al. reported that the exchange-bias in Pt/IrMn/CoFeB stacks can be controlled by SOT, which comes from Pt-layer-generated spin currents.<sup>[44]</sup> So one can expect that SOT-tunable multilevel-stable remanence states may be realized in Pt/IrMn/CoFeB stacks after further optimization of the device structure. In that case, it is possible to implement the Pt/IrMn/CoFeB stacks as the free layer in MTJs

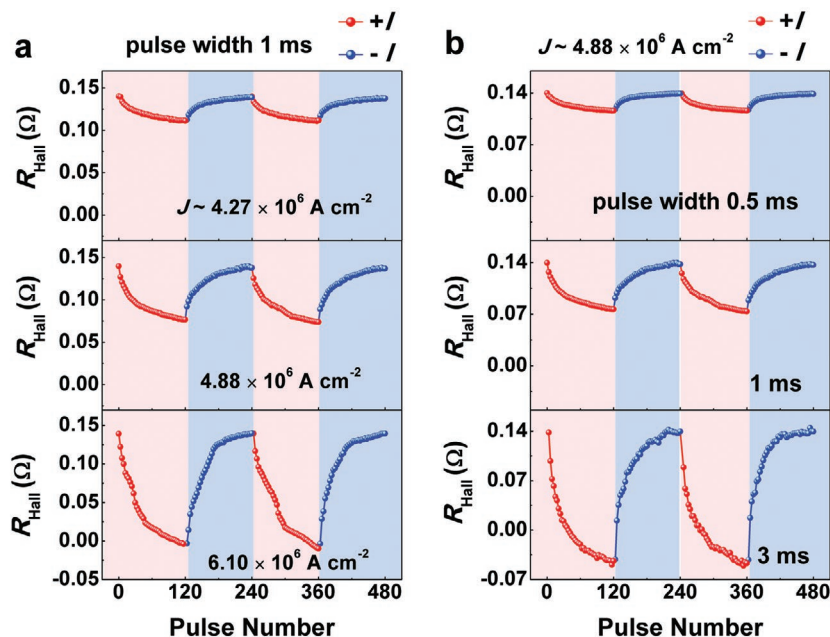


**Figure 5.** Dependence of the Hall resistance  $R_{\text{Hall}}$  on the programming consecutive current pulses under  $H_x = +500$  Oe. a)  $R_{\text{Hall}}$  responses to successive current pulses with positive polarity (red points) and negative polarity (blue points) for different current amplitudes with fixed pulse width of 1 ms. b)  $R_{\text{Hall}}$  responses to successive current pulses with positive polarity (red points) and negative polarity (blue points) for different pulse widths with fixed current amplitude  $J \approx 4.88 \times 10^6 \text{ A cm}^{-2}$ .

with an MgO tunneling barrier to realize multilevel states and large tunnel magnetoresistance (TMR) signal. Accordingly, the output signal that represents the multilevel states in MTJs will move from the anomalous Hall resistance to an immediate response in the possible larger TMR variation. Regarding to the elimination of the assistance field in SOT-tailored magnetic states, there are many methods that could be used to realize the field-free SOT switching in perpendicularly magnetized materials, such as by introducing a lateral structural asymmetry,<sup>[45,46]</sup> engineering a tilted anisotropy,<sup>[47]</sup> using interlayer exchange coupling,<sup>[36,48]</sup> and even using a magnetic hard mask in the fabrication of SOT-based MRAM.<sup>[49]</sup> Furthermore, although the multilevel remanence states driven by SOT is achieved in a micron-sized device in this work, the conclusion may be extended to the nanometer-sized devices based on the previous reports about the double-biased loops observed in the nanometer scale.<sup>[23,37]</sup> Thus, it may enable multilevel applications with high output signal, high density, and low power consumption characteristics for data storage and neuromorphic computing in exchange-biased systems.

### 3. Conclusion

In conclusion, SOT is demonstrated to be a promising approach to engineer the double-biased hysteresis loops in exchange-biased HM/FM/AFM systems. The heights of the positive and negative sub-loops can be tuned by the different amplitudes of current density ( $J$ ) and/or in-plane field  $H_x$ . The remanent magnetic domains associated with the evolution of

double-biased loops tailored by SOT are observed via Kerr microscope, which demonstrates that the multilevel remanence can be realized through domain wall motion. The engineered double-biased hysteresis loops could be used in the multilevel stable storage, which is quite attractive in information industry, and in the artificial synapse device, which is indispensable for neuromorphic computing. Our results show a significant impact not only on the tailoring of exchange-bias through SOT, but also on the non-volatile multilevel storage and neuromorphic computing applications.

Recently, we noticed a work reporting the similar tunable double-biased loops in HM/FM/AFM system by spin-orbit torque and giving an outlook in application of multilevel states.<sup>[50]</sup>

### 4. Experimental Section

**Sample Preparation:** The film stacks Ta(2.6)/Pt(5.5)/Co(0.8)/Ir<sub>20</sub>Mn<sub>80</sub>(6.2)/Ta(1.3)/TaO<sub>x</sub> (1.6) (thickness in nm) were deposited on Corning glass substrates by direct current magnetron sputtering at room temperature with a base pressure below  $5.0 \times 10^{-5}$  Pa. The top Ta was prepared to prevent oxidation of IrMn, and TaO<sub>x</sub> layer was naturally

formed due to the air exposure. Then the films were patterned into 10  $\mu\text{m}$  wide Hall bars using standard lithography and argon ion milling techniques for magnetotransport measurements.

**Characterization and Measurement:** The thicknesses were probed via grazing incidence X-ray reflectivity measurements. The anomalous Hall resistance measurements were carried out with Keithley 6221 as the current source. For each Hall resistance, a constant 0.1 mA bias current was applied to read the Hall voltage. The magnetic domain images of Hall bars were observed using a Kerr microscope working in a differential mode. Firstly, a large magnetic field ( $H_z \approx +2800$  Oe) was applied out-of-plane and an image was taken as a reference image. Next, another image was taken after a large current pulse and bias field  $H_x = +500$  Oe to record the magnetic domain in remanent state. Then the two images were aligned and the reference image was subtracted from the other to generate the final domain pattern. The SOT efficiency was obtained by harmonic Hall voltage measurements using an Analog-Digital/Digital-Analog data acquisition card with a sinusoidal current. All the above experiments were performed at room temperature. Several Hall bars were measured with the consistent results.

### Supporting Information

Supporting Information is available from the Wiley Online Library or from the author.

### Acknowledgements

This work was supported by the National Natural Science Foundation of China (Nos. 51671098, 11674143, 91963201), the Program for Changjiang Scholars and Innovative Research Team in University PCSIRT (No. IRT16R35) and the Natural Science Foundation of Gansu Province (No. 17J5RA210).



## Conflict of Interest

The authors declare no conflict of interest.

## Keywords

artificial synapses, double-biased hysteresis loops, exchange-bias, multilevel switching, spin-orbit torque

Received: November 1, 2019

Revised: January 11, 2020

Published online:

- [1] T.-S. Jung, Y.-J. Choi, K.-D. Suh, B.-H. Suh, J.-K. Kim, Y.-H. Lim, Y.-N. Koh, J.-W. Park, K.-J. Lee, J.-H. Park, K.-T. Park, J.-R. Kim, J.-H. Yi, H.-K. Lim, *IEEE J. Solid-State Circuits* **1996**, 31, 1575.
- [2] D. Lee, S. M. Yang, T. H. Kim, B. C. Jeon, Y. S. Kim, J.-G. Yoon, H. N. Lee, S. H. Baek, C. B. Eom, T. W. Noh, *Adv. Mater.* **2012**, 24, 402.
- [3] A. B. K. Chen, B. J. Choi, X. Yang, I. W. Chen, *Adv. Funct. Mater.* **2012**, 22, 546.
- [4] S. H. Jo, T. Chang, I. Ebong, B. B. Bhadviya, P. Mazumder, W. Lu, *Nano Lett.* **2010**, 10, 1297.
- [5] D. Kuzum, R. G. D. Jeyasingh, B. Lee, H.-S. P. Wong, *Nano Lett.* **2012**, 12, 2179.
- [6] T. Hasegawa, T. Ohno, K. Terabe, T. Tsuruoka, T. Nakayama, J. K. Gimzewski, M. Aono, *Adv. Mater.* **2010**, 22, 1831.
- [7] D. B. Strukov, G. S. Snider, D. R. Stewart, R. S. Williams, *Nature* **2008**, 453, 80.
- [8] P. Wadley, B. Howells, J. Železný, C. Andrews, V. Hills, R. P. Campion, V. Novák, K. Olejník, F. Maccheronzi, S. S. Dhesi, S. Y. Martin, T. Wagner, J. Wunderlich, F. Freimuth, Y. Mokrousov, J. Kuneš, J. S. Chauhan, M. J. Grzybowski, A. W. Rushforth, K. W. Edmonds, B. L. Gallagher, T. Jungwirth, *Science* **2016**, 351, 587.
- [9] D. Krieger, K. Výborný, K. Olejník, H. Reichlová, V. Novák, X. Marti, J. Gazquez, V. Saidl, P. Němec, V. V. Volobuev, G. Springholz, V. Holý, T. Jungwirth, *Nat. Commun.* **2016**, 7, 11623.
- [10] J. Železný, P. Wadley, K. Olejník, A. Hoffmann, H. Ohno, *Nat. Phys.* **2018**, 14, 220.
- [11] L. Liu, Q. J. Lee, T. J. Gudmundsen, D. C. Ralph, R. A. Buhrman, *Phys. Rev. Lett.* **2012**, 109, 096602.
- [12] S. Emori, U. Bauer, S.-M. Ahn, E. Martinez, G. S. D. Beach, *Nat. Mater.* **2013**, 12, 611.
- [13] G. Yu, P. Upadhyaya, K. L. Wong, W. Jiang, J. G. Alzate, J. Tang, P. K. Amiri, K. L. Wang, *Phys. Rev. B* **2014**, 89, 104421.
- [14] S. Zhang, S. Luo, N. Xu, Q. Zou, M. Song, J. Yun, Q. Luo, Z. Guo, R. Li, W. Tian, X. Li, H. Zhou, H. Chen, Y. Zhang, X. Yang, W. Jiang, K. Shen, J. Hong, Z. Yuan, L. Xi, K. Xia, S. Salahuddin, B. Dieny, L. You, *Adv. Electron. Mater.* **2019**, 5, 1800782.
- [15] Y. Cao, A. W. Rushforth, Y. Sheng, H. Zheng, K. Wang, *Adv. Funct. Mater.* **2019**, 29, 1808104.
- [16] W. H. Meiklejohn, C. P. Bean, *Phys. Rev.* **1956**, 102, 1413.
- [17] W. H. Meiklejohn, *J. Appl. Phys.* **1962**, 33, 1328.
- [18] J. Nogués, I. K. Schuller, *J. Magn. Magn. Mater.* **1999**, 192, 203.
- [19] A. E. Berkowitz, K. Takano, *J. Magn. Magn. Mater.* **1999**, 200, 552.
- [20] N. J. Gökemeijer, C. L. Chien, *J. Appl. Phys.* **1999**, 85, 5516.
- [21] I. V. Roshchin, O. Petravic, R. Morales, Z.-P. Li, X. Batlle, I. K. Schuller, *Europhys. Lett.* **2005**, 71, 297.
- [22] S. Brück, J. Sort, V. Baltz, S. Suriñach, J. S. Muñoz, B. Dieny, M. D. Baró, J. Nogués, *Adv. Mater.* **2005**, 17, 2978.
- [23] O. Petravic, Z.-P. Li, I. V. Roshchin, M. Viret, R. Morales, X. Batlle, I. K. Schuller, *Appl. Phys. Lett.* **2005**, 87, 222509.
- [24] W. Feng, N.-Y. Jiang, S.-D. Huang, H.-M. Chen, C.-W. Cheng, G. Chern, C.-C. Yu, *J. Appl. Phys.* **2012**, 111, 033904.
- [25] S. Chen, H. Zhao, G. Wang, Z. Zhang, B. Ma, Q. Y. Jin, *Thin Solid Films* **2013**, 534, 553.
- [26] I. M. Miron, K. Garello, G. Gaudin, P.-J. Zermatten, M. V. Costache, S. Auffret, S. Bandiera, B. Rodmacq, A. Schuhl, P. Gambardella, *Nature* **2011**, 476, 189.
- [27] S. Fukami, C. Zhang, S. DuttaGupta, A. Kurenkov, H. Ohno, *Nat. Mater.* **2016**, 15, 535.
- [28] K. Cai, M. Yang, H. Ju, S. Wang, Y. Ji, B. Li, K. W. Edmonds, Y. Sheng, B. Zhang, N. Zhang, S. Liu, H. Zheng, K. Wang, *Nat. Mater.* **2017**, 16, 712.
- [29] D. Li, S. Chen, Y. Zuo, J. Yun, B. Cui, K. Wu, X. Guo, D. Yang, J. Wang, L. Xi, *Sci. Rep.* **2018**, 8, 12959.
- [30] M. Yang, Y. Deng, Z. Wu, K. Cai, K. W. Edmonds, Y. Li, Y. Sheng, S. Wang, Y. Cui, J. Luo, Y. Ji, H.-Z. Zheng, K. Wang, *IEEE Electron Device Lett.* **2019**, 40, 1554.
- [31] P.-H. Lin, B.-Y. Yang, M.-H. Tsai, P.-C. Chen, K.-F. Huang, H.-H. Lin, C.-H. Lai, *Nat. Mater.* **2019**, 18, 335.
- [32] M. Björck, G. Andersson, *J. Appl. Crystallogr.* **2007**, 40, 1174.
- [33] J. Yun, Y. Zuo, J. Mao, M. Chang, S. Zhang, J. Liu, L. Xi, *Appl. Phys. Lett.* **2019**, 115, 032404.
- [34] A. Hubert, R. Schäfer, *Magnetic Domains: The Analysis of Magnetic Microstructures*, Springer, New York **1998**.
- [35] J. Yun, D. Li, B. Cui, X. Guo, K. Wu, X. Zhang, Y. Wang, J. Mao, Y. Zuo, L. Xi, *J. Phys. D: Appl. Phys.* **2018**, 51, 155001.
- [36] A. van den Brink, G. Vermijs, A. Solignac, J. Koo, J. T. Kohlhepp, H. J. M. Swagten, B. Koopmans, *Nat. Commun.* **2016**, 7, 10854.
- [37] G. Malinowski, M. Albrecht, I. L. Guhr, J. M. D. Coey, S. van Dijken, *Phys. Rev. B* **2007**, 75, 012413.
- [38] S. Brems, K. Temst, C. V. Haesendonck, *Phys. Rev. Lett.* **2007**, 99, 067201.
- [39] X. P. Qiu, D. Z. Yang, S. M. Zhou, R. Chantrell, K. O'Grady, U. Nowak, J. Du, X. J. Bai, L. Sun, *Phys. Rev. Lett.* **2008**, 101, 147207.
- [40] S. Lequeux, J. Sampaio, V. Cros, K. Yakushiji, A. Fukushima, R. Matsumoto, H. Kubota, S. Yuasa, J. Grollier, *Sci. Rep.* **2016**, 6, 31510.
- [41] A. Kurenkov, S. DuttaGupta, C. Zhang, S. Fukami, Y. Horio, H. Ohno, *Adv. Mater.* **2019**, 31, 1900636.
- [42] H. Markram, J. Lübke, M. Frotscher, B. Sakmann, *Science* **1997**, 275, 213.
- [43] J.-X. Shen, D.-S. Shang, Y.-S. Chai, S.-G. Wang, B.-G. Shen, Y. Sun, *Adv. Mater.* **2018**, 30, 1706717.
- [44] H.-J. Kim, S.-G. Je, D.-H. Jung, K.-S. Lee, J.-I. Hong, *Appl. Phys. Lett.* **2019**, 115, 022401.
- [45] G. Yu, P. Upadhyaya, Y. Fan, J. G. Alzate, W. Jiang, K. L. Wong, S. Takei, S. A. Bender, L.-T. Chang, Y. Jiang, M. Lang, J. Tang, Y. Wang, Y. Tserkovnyak, P. K. Amiri, K. L. Wang, *Nat. Nanotechnol.* **2014**, 9, 548.
- [46] B. Cui, H. Wu, D. Li, S. A. Razavi, D. Wu, K. L. Wong, M. Chang, M. Gao, Y. Zuo, L. Xi, K. L. Wang, *ACS Appl. Mater. Interfaces* **2019**, 11, 39369.
- [47] L. You, O. J. Lee, D. Bhowmik, D. Labanowski, J. Hong, J. Bokor, S. Salahuddin, *Proc. Natl. Acad. Sci. U. S. A.* **2015**, 112, 10310.
- [48] Y.-C. Lau, D. Betto, K. Rode, J. M. D. Coey, P. Stamenov, *Nat. Nanotechnol.* **2016**, 11, 758.
- [49] K. Garello, F. Yasin, H. Hody, S. Couet, L. Souriau, S. H. Sharifi, J. Swerts, R. Carpenter, S. Rao, W. Kim, J. Wu, K. K. V. Sethu, M. Pak, N. Jossart, D. Crotti, A. Furnémont, G. S. Kar, arXiv:1907.08012, **2019**.
- [50] X. H. Liu, K. W. Edmonds, Z. P. Zhou, K. Y. Wang, arXiv:1910.12445, **2019**.